

# HOT MOLECULAR GAS IN THE NUCLEAR REGION OF IC 342

María Montero-Castaño<sup>1,2</sup>, Robeson M. Herrnstein<sup>3</sup> and Paul T.P. Ho<sup>1,4</sup>

## ABSTRACT

We present the first interferometric detection of extragalactic  $\text{NH}_3(6,6)$  emission in the nearby galaxy IC 342 made using the VLA<sup>5</sup>. The data have a resolution of  $7.8'' \times 5.0''$  and trace hot ( $T \sim 412$  K) and dense ( $> 10^4 \text{ cm}^{-3}$ ) molecular gas. We have covered a  $170'' \times 300''$  area, and detect two very strong line emission peaks, likely associated with the two strongest star formation regions of the central part of the galaxy. We compare these emission peaks to CO (1-0) and (2-1) emission data, which are the most abundant CO transitions and trace spatially extended emission. The  $\text{NH}_3(6,6)$  emission is also compared to emission data from three high-density, nitrogen bearing tracers:  $\text{HNC}(1-0)$ ,  $\text{HC}_3\text{N}(10-9)$  and  $\text{N}_2\text{H}^+$ . Our results suggest that the molecular mass in the nuclear region of IC 342 has at least two different components, a dense and cold component and a less dense and hotter component.

*Subject headings:* nearby galaxies: general — molecular clouds: individual (IC 342)

---

<sup>1</sup>Harvard-Smithsonian Center for Astrophysics, 60 Garden St., Cambridge, MA 02138, mmontero@cfa.harvard.edu, pho@cfa.harvard.edu

<sup>2</sup>Departamento de Astrofísica, Facultad de Ciencias Físicas, Universidad Complutense de Madrid, 28040-Madrid, Spain

<sup>3</sup>Department of Astronomy, Columbia University, 550 West 120th St., New York, NY 10027, herrnstein@astro.columbia.edu

<sup>4</sup>Academia Sinica Institute of Astronomy and Astrophysics, Taipei, Taiwan

<sup>5</sup>The National Radio Astronomy Observatory is a facility of the National Science Foundation operated under cooperative agreement by Associated Universities, Inc.

<sup>6</sup>This research has made use of the NASA/IPAC Extragalactic Database (NED) which is operated by the Jet Propulsion Laboratory, California Institute of Technology, under contract with the National Aeronautics and Space Administration

## 1. Introduction

IC 342, a late-type spiral galaxy (Scd), is one of the closest galaxies to the Milky Way, located only  $\sim 3.3$  Mpc away (Saha et al. 2002; Karachentsev 2005) ( $1''$  corresponds to 16 pc). The physical properties of its molecular clouds, its infrared luminosity, and the presence of a nuclear stellar cluster (Hüttemeister et al. 1995; Schulz et al. 2001) make IC 342 similar to the Milky Way in many ways. Because of its proximity to the Galactic equator, IC 342 is a faint optical source. However, it is a very rich source of molecular emission, and has been studied in numerous molecular tracers. Furthermore, IC 342 is nearly face-on, minimizing line broadening due to galactic rotation, thereby maximizing line intensity. This orientation makes IC 342 useful for Milky Way-like studies.

IC 342 has a high concentration of molecular gas within the inner 1 kpc, especially within 250 pc of the nucleus (Israel & Baas 2003). Inflow along a large-scale stellar bar (Schinnerer et al. 2003) has been proposed to explain the large quantity of gas in the nucleus. An S-shaped bar in the molecular gas (the “mini-spiral”), has been clearly detected in the nuclear region in CO(1-0) (Helfer et al. 2003) as well as in NIR observations (Böker et al. 1997). The mini-spiral is oriented in the north-south direction, and it is apparently unrelated to the spiral arms located further out in the disk (Lo et al. 1984). The two arms of the mini-spiral meet in a ring composed of dense gas (Ishizuki et al. 1990; Meier & Turner 2001). This ring,  $\sim 4''$  in radius, surrounds a central stellar cluster that occupies the central 80 pc of the galaxy (Turner & Hurt 1992; Böker et al. 1997). The central stellar cluster is non-axisymmetric, with a north-south elongation, which is believed to be caused by the presence of a nuclear stellar bar with a major axis diameter of  $\sim 13''$  (Böker et al. 1997). The nuclear bar creates the ring-like structure at  $4''$ , an Inner Lindblad Resonance (ILR) (Böker et al. 1997). Inside the ring, the abundance decreases for all the molecular tracers studied to date (Meier & Turner 2005).

Current star formation activity in the nucleus of IC 342 is dominated by two bright HII regions  $\sim 4''$  west and east of the nuclear cluster. These star formation regions are  $\sim 5$  Myr old. The central cluster, which is composed of young and massive supergiants, does not show evidence for current star formation (Böker et al. 1997).

High-resolution HCN(1-0) studies by Downes et al. (1992) have shown the presence of five giant molecular clouds (GMCs) in IC 342 (GMCs A, B, C, D, and E). These GMCs have sizes from 20 to 40 pc, masses of  $\sim 10^6 M_{\odot}$  and average molecular densities of  $\sim 10^4 \text{ cm}^{-3}$  (Schulz et al. 2001). Each GMC appears to be composed of multiple small, dense clouds (Meier & Turner 2001), which have densities of  $\sim 10^6 \text{ cm}^{-3}$  (Schulz et al. 2001). Downes et al. (1992), Helfer & Blitz (1993) and Jackson et al. (1996) have shown that the distribution of GMCs extends close to the nucleus (within a distance of 100 pc) and well inside the tidal

limit. The region occupied by these GMCs includes both the arms of the mini-spiral and the ring.

GMCs A, B and C are located in the central ring, whereas GMCs D and E are in the northern arm and southern arm of the mini-spiral, respectively. GMCs B and C are situated where the arms of the mini-spiral meet the ring, and may be related to the young star formation regions found there (the two HII regions mentioned above). High-resolution studies of C<sup>18</sup>O by Meier & Turner (2001) show that GMC B is the warmest GMC in the central region. GMC A is the closest to the nucleus, but it does not show strong star formation. GMC D also does not show strong star formation, although it is located alongside the northern arm where Turner & Hurt (1992) detected large quantities of molecular gas with inward motions. GMC N, as noted by Meier & Turner (2005), is located close to GMCs A and B, in the molecular ring. It has only been detected in nitrogen bearing molecules.

The GMCs are very warm, with a temperature of 50 to 70 K measured using HCN(1-0) (Downes et al. (1992)). However, more recent CO(2-1) observations by Meier et al. (2000) have shown that most of the gas within the GMCs has a temperature of only 10-20 K. This cool gas is surrounded by much hotter Photon Dominated Regions (PDRs) with temperatures that reach 50 K. The ionization of the PDRs may be produced by the central nuclear cluster, rather than by the HII regions close to GMCs B and C (Meier & Turner 2005).

The GMCs associated with the nucleus of IC 342 have been the subject of numerous molecular line studies. However, few observations have been made in the rotation inversion transitions of NH<sub>3</sub>. NH<sub>3</sub> is a good probe of the physical conditions in molecular clouds for many reasons. The large number of transitions concentrated around  $\sim 1.3$  cm means that multiple ammonia lines can be detected with the same receiver on the same telescope, thereby circumventing cross calibration problems. Moreover, measuring two emission lines allows us to calculate the rotational temperature of the gas (Ho & Martin 1983). Also, due to its high dipole moment, a density of  $\sim 10^4$  cm<sup>-3</sup> is necessary to excite NH<sub>3</sub>, making it an excellent high-density gas tracer.

The first detection of extragalactic NH<sub>3</sub> emission was made in IC 342 by Martin & Ho (1979) using the 100m Effelsberg telescope of the Max-Planck-Institut für Radioastronomie. Numerous studies, both with interferometers and single-dish antennas, have been carried out since then in IC 342 (Ho, Martin, & Ruf 1982; Ho & Martin 1983; Martin & Ho 1986; Ho et al. 1990; Mauersberger et al. 2003), as well as in other galaxies (Henkel et al. 2000; Weiß et al. 2001; Takano et al. 2002; Beuther et al. 2005; Ott et al. 2005). However, the only previous study of NH<sub>3</sub>(6,6) in IC 342 was made by Mauersberger et al. (2003) using the 100m Effelsberg telescope. This study detected the presence of warm gas ( $> 150$  K) in the center of IC 342. In particular, they found a high abundance of NH<sub>3</sub>(6,6) ( $N_{66} = 3.2 \times 10^{12}$  cm<sup>-2</sup>),

which has an excitation energy above ground of 412 K. This study also suggested the presence of multiple components with different temperatures within the beam. However, due to the large beam ( $38''$  for  $\text{NH}_3(6,6)$ ) for these single-dish data, the multiple components could not be separated.

We have conducted a study of  $\text{NH}_3(6,6)$  using the VLA in order to resolve the structure of the hot dense gas in the nucleus of IC 342. Our interferometric observations produce a much smaller beam ( $7.8'' \times 5.0''$ ), allowing us to separate the emission from different structures present in the nucleus of IC 342. In addition to studying the molecular structure of the IC 342 nuclear region, we also relate our data to the center of the Milky Way. As previously mentioned, IC 342 is a perfect candidate for Milky Way-like studies. Interferometric observations of  $\text{NH}_3(6,6)$  at the Galactic Center have shown that there is a large concentration of high density hot gas surrounding Sgr A\* (Herrnstein & Ho 2002, 2005). Therefore, the study of the nuclear region of IC 342 is not only important in itself, but it also provides an excellent opportunity to investigate the same processes that take place in our own Galactic Center.

## 2. Observations

Observations of  $\text{NH}_3(6,6)$  ( $\nu = 25.056025$  GHz) were made with the NRAO Very Large Array (VLA<sup>5</sup>) in the D configuration on 2003 February 15 and 16. The pointing was centered on  $\alpha_{2000} = 03^h46^m48.7^s$ ,  $\delta_{2000} = 68^\circ05'46.7''$ . The data consisted of a 25 MHz bandwidth divided into 15 spectral channels with a velocity resolution of  $9.3 \text{ km s}^{-1}$ . The velocity coverage was from  $-30 \text{ km s}^{-1}$  to  $+110 \text{ km s}^{-1}$ , centered on  $v_{LSR} = 40 \text{ km s}^{-1}$ . Channels 1, 14 and 15 were removed from the data because of low sensitivity due to the roll off in the passband response. Channels 2 and 3 were used for continuum subtraction, which was performed in the uv plane, thus resulting in an effective velocity coverage from  $0 \text{ km s}^{-1}$  to  $90 \text{ km s}^{-1}$ . The fact that the continuum subtraction has been performed using channels from only one side of the line does not affect the final result since the bandpass was calibrated by observing 0319+415 (3C84).

The data were calibrated using the NRAO Astronomical Imaging Processing System (AIPS). The total on-source integration time was  $\sim 7$  hours. The flux calibrator was 0137+331 (3C48) with an assumed flux of 0.99 Jy at 1.3 cm. The phase calibrator was 0228+673, with a measured flux of  $1.04 \pm 0.01$  Jy. We performed phase-only self-calibration to correct for atmospheric fluctuations on short time-scales. The self-calibration was done on the broadband continuum data (the average of the inner 75% of the 25 MHz window), and the results were applied to the line data. Final deconvolution was performed using IMAGR.

The overall improvement in RMS noise due to self-calibration was about a factor of 2. The final RMS noise per channel is  $0.3 \text{ mJy Beam}^{-1}$  and the overall achieved RMS sensitivity is  $3.6 \text{ mJy Beam}^{-1} \text{ km s}^{-1}$ . Natural weighting of the uv data produced an image with a synthesized beam of  $7.8'' \times 5.0''$  with a position angle of  $64^\circ$ . The integrated intensity map was produced using the MOMNT task with a minimum flux cutoff of  $0.4 \text{ mJy}$ . The absolute positional accuracy is limited by phase noise, and is on the order of  $1''$ .

### 3. Results

We detect and resolve the extended  $\text{NH}_3(6,6)$  emission from IC 342 (figure 1). Three line emission peaks are clearly visible in our results, marked by numbers 1-3 on figure 1. Peaks 1 and 2 appear to be embedded in a single, extended molecular structure. The third peak, which has not been previously observed in any molecular tracer, is isolated. Comparing the line emission map with the continuum map (in contours and false colors, respectively, in figure 1), we find that peak 2 corresponds to the continuum emission peak, which marks the location of a strong heating source as well as the nucleus of IC 342 (Downes et al. 1992). Throughout this paper, peak 1 will be referred to as the *(6,6) peak*, peak 2 as the *continuum peak*, and peak 3 as the *west peak*.

We compared our  $\text{NH}_3(6,6)$  flux with the single-dish data from Mauersberger et al. (2003). Because the beam size for the 100m Effelsberg telescope is  $38''$ , all three of our  $\text{NH}_3(6,6)$  peaks are well within the Effelsberg beam. From Mauersberger et al. (2003), the single-dish flux is  $4.5 \times 10^{-3} \text{ Jy Beam}^{-1}$ , while the sum of the fluxes detected for the three  $\text{NH}_3(6,6)$  peaks presented in this paper is  $4.6 \times 10^{-3} \text{ Jy Beam}^{-1}$ . Therefore, there is no missing flux, and all emission detected in the single-dish data must originate in clouds with size scales smaller than  $\sim 8''$ .

Because the relative locations of the  $\text{NH}_3(6,6)$  emission peaks and the GMCs may provide a clue to the behavior of material near the nucleus of IC 342, we overlay the positions of the 6 GMCs on our  $\text{NH}_3(6,6)$  map (GMCs A, B, C, D, E and N in figure 2). We plot the spectra at the positions of our three peaks and the 6 GMCs. For comparison, we also plot spectra taken from three random, emission-free positions (figure 3).

In order to investigate the physical conditions in the  $\text{NH}_3(6,6)$  clouds that we observe, we also compare our  $\text{NH}_3(6,6)$  map to  $\text{HNC}(1-0)$ ,  $\text{HC}_3\text{N}(10-9)$ ,  $\text{N}_2\text{H}^+(1-0)$  (Meier & Turner 2005),  $\text{CO}(1-0)$  (Helfer et al. 2003), and  $\text{CO}(2-1)$  (Schinnerer et al. 2003). We have chosen these five molecular lines for different reasons.  $\text{HNC}$ ,  $\text{HC}_3\text{N}$  and  $\text{N}_2\text{H}^+$  have proved to be high-density tracers. Moreover, these molecules are nitrogen bearing like  $\text{NH}_3$ . Comparing

the results from  $\text{HC}_3\text{N}$ ,  $\text{HNC}$  and  $\text{N}_2\text{H}^+$  with  $\text{NH}_3$ , we can determine whether GMC N is also an emission peak in  $\text{NH}_3$ .

$\text{CO}$  is second only to  $\text{H}_2$  in terms of abundance in the interstellar medium. However,  $\text{H}_2$  cannot be directly studied because of the lack of a dipole moment. We compare our  $\text{NH}_3(6,6)$  data to  $\text{CO}(2-1)$  and  $(1-0)$ , which, because of their low excitation requirements, are the molecular tracers that detect more extended emission in IC 342. Most of the  $\text{CO}(1-0)$  emission comes from the extended ridges of the mini-spiral, but not directly from the GMCs embedded in it (Downes et al. 1992). In contrast,  $\text{CO}(2-1)$ , at twice the excitation above ground, is detected in warmer gas than  $\text{CO}(1-0)$ . As mentioned before, Meier et al. (2000) have found most of the gas inside the GMCs to be colder than the gas outside of them, since the GMCs are surrounded by PDRs. Thus, it is not surprising that the warmer  $\text{CO}(2-1)$  is detected in the thin outer layers of the GMCs where they are heated from outside by UV photons (Turner et al. 1993). Therefore, the comparison with  $\text{NH}_3(6,6)$  could provide some clue as to the kind of gas traced by this highly excited transition. We expect to find  $\text{NH}_3(6,6)$  concentrated in the areas where  $\text{CO}(1-0)$  is weaker and inside the GMCs traced by  $\text{CO}(2-1)$ . A gas distribution of this sort would reflect the fact that  $\text{NH}_3$  is optically thin, while  $\text{CO}$  is optically thick, and that the gas distribution depends on density. Therefore, even though the hotter  $\text{CO}$  has been detected outside of the GMCs instead of inside, we expect the optically thin and dense  $\text{NH}_3$  to be found well inside the GMCs.

Because the different molecular lines have been measured using different telescopes, we have resampled the maps with the same size pixels, in order to allow a proper registration for direct comparison. We did not convolve the maps, choosing to keep the full resolution of each map. However, most of the maps we use for comparison in fact have a very similar angular resolution to our data. We use the latest  $\text{HNC}(1-0)$ ,  $\text{HC}_3\text{N}(10-9)$  and  $\text{N}_2\text{H}^+(1-0)$  results from Meier & Turner (2005). These three molecular lines have been measured using the Owens Valley Radio Observatory (OVRO) and have an angular resolution of 5-6'' with a positional accuracy of  $\sim 1''$ . The  $\text{CO}(2-1)$  map by Schinnerer et al. (2003) was also made using OVRO, but the angular resolution is 1.2'' with a positional uncertainty of less than 0.1''. Matching the angular resolution of  $\text{CO}(2-1)$  to our  $\text{NH}_3$  data was not useful because the detected structures would be smoothed away.  $\text{CO}(1-0)$  has been measured using the Berkeley-Illinois-Maryland Array (BIMA) together with the 12m NRAO antenna (Helfer et al. 2003). The angular resolution of 5.6'' is similar to the resolution of our VLA data. The  $\text{CO}(1-0)$  data have a positional accuracy of  $\sim 0.4''$ . Only the  $\text{CO}(1-0)$  data include short spacing information, and are thus sensitive to large-scale structure. Therefore, the flux associated with the other molecular tracers must be assumed to be a lower limit. The lack of short spacings does not appear to be as important for  $\text{NH}_3(6,6)$  as there is no missing flux as compared to single-dish measurements. Nevertheless, some caution must be applied

to detailed comparisons between molecules.

In order to understand the significance of the *west peak*, which is not detected in any of the other molecular lines, we also compare our results to a 6 cm continuum map from the VLA (C.-W. Tsai, private communication) (figure 9). The 6 cm continuum peak appears spatially coincident with our 1.3 cm continuum map (figure 10). Therefore, we are confident that the features we observe in  $\text{NH}_3(6,6)$  are well placed in comparison with the 6 cm map, i.e. the positional accuracy is reliable.

Finally, it would be very useful to compare the  $\text{NH}_3(6,6)$  emission to emission from other metastable transitions of  $\text{NH}_3$ . Comparing our  $\text{NH}_3(6,6)$  map with the  $\text{NH}_3(1,1)$  and  $(2,2)$  maps by Ho et al. (1990) we find that, in general, the detected features on the three maps are remarkably different. Since the lower excitation lines are sensitive to colder gas, the  $\text{NH}_3(1,1)$  and  $(2,2)$  maps appear to trace the more extended emission, such as the mini-spiral, and GMC D. However, the emission in these lower lines seems to “avoid” the position where the *continuum peak* is located, whereas the  $\text{NH}_3(6,6)$  emission is very strong in that location. Ho et al. (1990) associated the weakness of  $\text{NH}_3(1,1)$  and  $(2,2)$  toward the continuum source either with photoionization or high temperatures present in the nuclear region. Because of the detection of  $\text{NH}_3(6,6)$ , which is at 412 K above ground, the second scenario is indeed the most plausible explanation. More recent results in  $\text{NH}_3(1,1)$  and  $(2,2)$  are consistent with the earlier results (M. Lebrón, private communication).

Below, we discuss the three  $\text{NH}_3(6,6)$  peaks in turn.

### 3.1. (6,6) peak

When comparing the  $\text{NH}_3(6,6)$  map with the positions of the GMCs, we notice that the  $(6,6)$  *peak* is remarkably close to GMC C (figure 2). The two positions are in fact coincident to within the absolute positional uncertainties of the  $\text{NH}_3$  map. We conclude that the  $(6,6)$  *peak* and GMC C are likely the same structure. Previous studies have demonstrated that the strongest star formation areas in the central region of IC 342 are GMCs B and C, which are both located where the arms meet the ring. Therefore,  $\text{NH}_3(6,6)$  traces areas where the star formation activity has been enhanced.

The  $\text{HC}_3\text{N}(10-9)$  emission from Meier & Turner (2005) has a structure similar to that of the  $\text{NH}_3(6,6)$  emission (figure 4). In both maps, the strongest line emission is found at the position of the  $(6,6)$  *peak*. We compare the line profiles detected in  $\text{HC}_3\text{N}(10-9)$  by Meier & Turner (2005) with that in  $\text{NH}_3(6,6)$  at the position of the GMC that is closer to our detected peak (GMC C) and we find that they have very similar velocities. Thus  $\text{HC}_3\text{N}(10-9)$  and

$\text{NH}_3(6,6)$  appear to trace the same high-density, high-temperature material.

When comparing the  $\text{NH}_3(6,6)$  results with those from the  $\text{HNC}(1-0)$  map by Meier & Turner (2005) we find that the emission of the GMC close to the position of the  $(6,6)$  peak (GMC C) is weaker than the emission arising from another region of the map (figure 5). The different behavior might indicate that  $\text{HNC}(1-0)$  is a density tracer while  $\text{NH}_3(6,6)$  is a better temperature tracer. In fact, Meier & Turner (2005) note that  $\text{HNC}$  is more strongly detected in areas of high volume density, not only high column density.

The distribution of  $\text{N}_2\text{H}^+(1-0)$  is very similar to that of  $\text{HNC}(1-0)$  (figure 6), although the  $\text{N}_2\text{H}^+(1-0)$  emission is slightly more extended towards the north, tracing the northern arm of the mini-spiral. The  $\text{N}_2\text{H}^+(1-0)$  emission peaks at the location of GMC N, which is not close to the  $(6,6)$  peak (see figure 1).  $\text{N}_2\text{H}^+$  is believed to trace dense quiescent gas (Womack et al. 1992). The lack of coincidence between the  $\text{N}_2\text{H}^+(1-0)$  and the  $\text{NH}_3(6,6)$  maps indicates that the ion is tracing the areas where the star formation seems to be less intense or non-existent, while the  $\text{NH}_3(6,6)$  is present in active star formation regions.

The  $(6,6)$  peak coincides with the  $\text{CO}(2-1)$  peak measured by Schinnerer et al. (2003) (figure 7). The  $\text{CO}(2-1)$  traces the eastern and western parts of the two molecular spiral arms where they form the molecular ring. The  $\text{NH}_3(6,6)$  appears to extend outside of the eastern arm, but the spatial coincidence is excellent when the different angular resolutions of the two data-sets are considered. This coincidence of  $\text{NH}_3(6,6)$  and  $\text{CO}(2-1)$  suggests that the gaseous material flowing inwards along the northern arm of the “mini-spiral” is interacting with the inner ring, heating GMC C, and therefore producing the  $\text{CO}(2-1)$  emission. This interaction may also be triggering a burst of star formation at the same location.

Like in the  $\text{CO}(2-1)$  map, the  $\text{NH}_3(6,6)$  peak appears to be offset by  $1''$  to the SE as compared to the  $\text{CO}(1-0)$  map by Helfer et al. (2003) (figure 8). In this case, the angular resolutions of the two maps are similar. The slight offset may not be significant given the absolute positional error of about  $1''$ . The  $\text{CO}(1-0)$  traces the more extended and colder gas that forms the S-shaped bar, whereas the  $\text{NH}_3(6,6)$  is more compact and detects the warmer material accumulated in the regions where the inflow from the bar meets the inner ring. However, the  $\text{NH}_3(6,6)$  and the  $\text{CO}(1-0)$  maps do seem to be well-correlated, since both main peaks are detected.

When comparing the  $\text{NH}_3(6,6)$  map with the 6 cm continuum map, we find that the  $(6,6)$  peak appears at the edge of the 6 cm continuum emission (figure 9). The 6 cm emission seems to have a “tail” that ends at the position of the  $(6,6)$  peak. However, there is no evidence for a diffuse continuum component in this area. Becklin et al. (1980) and Turner & Ho (1983) found that the 6 cm continuum map of the center of IC 342 was mainly



dominated by free-free thermal emission. However, in the northern part of the CNB where the  $(6,6)$  peak is located, the emission was mostly from synchrotron origin. Thus, there is synchrotron emission associated with the  $(6,6)$  peak, but not with its surroundings. A possible explanation for these observations could be that the  $(6,6)$  peak is located in the position of a very concentrated burst of star formation that has developed some supernovae, but no such activity has taken place outside of this position.

In summary, the presence of a strong star formation region where the  $(6,6)$  peak is located, and a comparison of the  $\text{NH}_3(6,6)$  distribution with other molecular lines, suggest that the  $(6,6)$  peak has the characteristics of a column density and temperature peak.

### 3.2. Continuum peak

The  $\text{NH}_3(6,6)$  continuum peak is offset by  $2''$ - $3''$  from GMCs B, A and N, which trace an arc around it (figure 2). This offset appears significant, especially since the  $\text{NH}_3(6,6)$  continuum peak coincides well with the 6 cm continuum peak (figure 9). When comparing GMC B and the continuum peak spectra, we notice that even though the continuum peak spectrum is stronger, the integrated intensity is very similar. As remarked before, GMC B is a very strong star formation area. On the other hand, no trace of star formation has been detected towards GMC A to date. The lack of a strong  $\text{NH}_3(6,6)$  detection at the position of GMC A supports the theory that there is no current star formation in this region. GMC A has a  $\text{NH}_3(6,6)$  spectrum only slightly more intense than the background emission-free spots (figure 3). We do not find a differentiated feature in the integrated intensity map where GMC N should be. However, the spectrum at this position is clearly above noise-level.

The  $\text{HC}_3\text{N}(10-9)$  map from Meier & Turner (2005) shows a peak near the continuum peak (figure 4). As in the  $\text{NH}_3(6,6)$  map, the continuum peak seems weaker than the  $(6,6)$  peak. Since GMC B, which seems to be the GMC closer to the continuum peak, is the warmest region of the nucleus of IC 342, the fact that  $\text{NH}_3(6,6)$  and  $\text{HC}_3\text{N}(10-9)$  are weaker at this point may suggest that the total column density is not a maximum at this position.

The continuum peak is offset by  $2''$  north of the secondary peak in  $\text{HC}_3\text{N}(10-9)$  and the primary peak detected in  $\text{HNC}(1-0)$  by Meier & Turner (2005) (figure 5). This offset appears to be significant. A similar offset between  $\text{NH}_3(6,6)$  and  $\text{N}_2\text{H}^+(1-0)$  is also observed. These results suggest that neither  $\text{HC}_3\text{N}(10-9)$  nor  $\text{HNC}(1-0)$  nor  $\text{N}_2\text{H}^+(1-0)$  are tracing a temperature peak, which is in fact better traced by  $\text{NH}_3(6,6)$ .

The continuum peak is a very weak feature in the  $\text{CO}(2-1)$  map (Schinnerer et al. 2003). Unlike  $\text{NH}_3(6,6)$ ,  $\text{CO}(2-1)$  does not detect the gas associated with the heating source located

at the *continuum peak*, but instead traces the gas surrounding it (figure 7).

The *continuum peak* also appears offset by  $3''$  from the secondary peak detected in the CO(1-0) map by Helfer et al. (2003) (figure 8). As in the  $\text{NH}_3(6,6)$  map, this secondary peak is weaker than the one that coincides with the  $(6,6)$  *peak*, and although the kind of gas traced by the two molecules have different temperatures, the overall structure has some similarities.

Finally, as expected, the *continuum peak* is located close to the 6 cm continuum emission peak (figure 9). The 6 cm continuum emission seems to trace an arc structure around the  $\text{NH}_3(6,6)$  *continuum peak* rather than being concentrated at that same spot. In this case, the angular resolution is different by a factor of 10. With higher resolution, the  $\text{NH}_3(6,6)$  emission could be even better correlated with the 6 cm continuum structure. The good correspondence with the radio continuum peak, and the offset of a few arcseconds relative to other molecular peaks which sample lower temperature gas, suggests that the  $\text{NH}_3(6,6)$  emission could be tracing a hot molecular component near the nucleus. Israel & Baas (2003) suggest that the nucleus of IC 342 has two different molecular mass components, a cold and dense component, which represents about one third of the total molecular mass, and a less dense and hotter component. A similar situation has also been observed in the center of the Milky Way. By looking at six  $\text{NH}_3$  metastable inversion transitions (from (1,1) to (6,6)) in the Galactic Center region ( $575 \text{ pc} \times 145 \text{ pc}$ ), Hüttemeister et al. (1993) find the distribution of the transition lines to differ from one another. While lower transition lines look similar, the higher transitions often look very different. In fact, Hüttemeister et al. (1993) find that molecular gas in the nuclear region of the Galaxy is best modeled as a mixture of hot ( $\sim 200 \text{ K}$ ) and cold ( $25 \text{ K}$ ) gas, in which 75% of the gas is in the cold component. This “two-temperature” structure continues to hold even within  $5 \text{ pc}$  of the nucleus (Herrnstein & Ho 2005). Furthermore, studies by Herrnstein & Ho (2002), with a similar velocity resolution to ours, find  $\text{NH}_3(6,6)$  to be clearly concentrated in the nucleus of the Milky Way. Obviously, the Galactic Center study refers to a much more concentrated and less massive material than the material detected in IC 342, given the different size-scales ( $2.7 \text{ kpc} \times 4.8 \text{ kpc}$  for IC 342,  $10 \text{ pc} \times 10 \text{ pc}$  for the Galactic Center). Therefore, the mechanism that drives the  $\text{NH}_3(6,6)$  in the nuclear region of IC 342, which is likely to be a star formation process, might be more extensive spatially than the mechanism that is working in the Galactic Center. Nevertheless, given the similar behaviour we find in the nuclear regions of IC 342 and the Galactic Center, this suggests that the *continuum peak* could be tracing the hot component present in the nucleus of IC 342, i.e. the *continuum peak* is a temperature peak.

### 3.3. West peak

The *west peak* has no counterpart in any other molecular line map that has been published to date. However, the careful reduction process that we have used gives us confidence to conclude that this structure is not a noise feature. In addition, the lack of a symmetric counterpart on the other side of the nucleus of IC 342 leads us to conclude that the *west peak* is unlikely a sidelobe effect. The *west peak* is not very strong, but it is a remarkable feature because it is detected over a wide velocity range. We compare the *west peak* spectrum to three randomly chosen noise-level spectra in figure 3. We find that, although weak, the overall flux level associated with the *west peak* is above the noise level.

The comparison of the  $\text{NH}_3(6,6)$  emission map with the latest VLA 6 cm continuum emission map from Ch.-W. Tsai (A and C configurations combined) shows no evidence of radiocontinuum emission at this location (figure 9).

The presence of  $\text{NH}_3(6,6)$  at positions where there have been no previous molecular detections has occurred elsewhere. In the Milky Way,  $\text{NH}_3(6,6)$  has been detected within 2 pc of the Galactic Center with no corresponding emission from other molecular tracers (Herrnstein & Ho 2002). This molecular emission (termed the “high-line-ratio-cloud”) is thought to be the result of absorption of low-energy transitions (in particular  $\text{NH}_3(1,1)$ , (2,2) and (3,3)) by cool material along the line-of-sight (Herrnstein & Ho 2005). Though the size scale of the Galactic Center emission ( $< 2$  pc) is much smaller than the size scales traced in our IC 342 data, it is possible that a similar geometrical effect could explain the lack of low-energy molecular emission associated with the IC 342 *west peak*.

### 3.4. Mass estimates

Since we have detected three different peaks, we separate the  $\text{NH}_3(6,6)$  structure into three different areas and calculate the mass in each.

Because we have only measured one transition line,  $\text{NH}_3(6,6)$ , we cannot directly calculate the excitation temperature of the gas. Theoretically, the  $\text{NH}_3(6,6)$  opacity could be measured using the hyperfine splitting of the  $\text{NH}_3(6,6)$  emission line. However, due to the weakness of the satellite lines (roughly 3% of the main hyperfine line for optically thin gas) and the large linewidths, this calculation is not possible for our data. We therefore assume optically thin emission ( $\tau \ll 1$ ) and also consider the source to fill the clean beam giving

$$T_{ex}\tau \cong T_b . \tag{1}$$

We can obtain the  $T_b$  directly from the line profile, using

$$T_b = \frac{\lambda^2}{2k\Omega} S_\nu, \quad (2)$$

where  $\lambda$  is the wavelength,  $k$  is Boltzmann's constant,  $\Omega$  the solid angle and  $S_\nu$  is the peak flux density.

The column density is calculated using

$$N_{JK} = 4.1 \times 10^{-20} \text{ cm}^{-2} \frac{\tau \nu T_{ex} \Delta v}{A_{10} k_{JK}}. \quad (3)$$

For  $\text{NH}_3(6,6)$ ,  $k_{66} = 0.969$ ,  $A_{10} = 3.38 \times 10^{-7} \text{ s}^{-1}$ , and  $\nu = 25.056 \text{ GHz}$  (Herrnstein 2003).

Once we know the value of the column density, we obtain the molecular mass through the following equation:

$$M_{H_2} = N_{66} \times Area \times \frac{1}{f_{66}} \times \left[ \frac{N(H_2)}{N(NH_3)} \right] \times m_{H_2}, \quad (4)$$

where  $f_{66}$  is the fraction of  $\text{NH}_3$  molecules in the (6,6) state, and is on the order of 0.1 for temperatures higher than 150 K. We use  $\frac{N(H_2)}{N(NH_3)} = 10^{7.5}$  from Mauersberger et al. (2003), which is the relative abundance of  $\text{H}_2$  to  $\text{NH}_3$  in fairly warm environments ( $T > 150 \text{ K}$ ).

The resulting mass estimates for each  $\text{NH}_3(6,6)$  peak are given in table 1.

We detect a total warm gas mass of  $8.2 \times 10^6 M_\odot$ , clearly much larger than the amount of warm gas mass detected in the interior of the Galactic Center Circumnuclear Disk by Herrnstein & Ho (2002),  $10^4 M_\odot$  (inner 1.5 pc around Sgr A\*). Rigopoulou et al. (2002) reported a warm mass of  $5.0 \times 10^6 M_\odot$  measuring the quadrupole transition lines of  $\text{H}_2$  using the Infrared Space Observatory (ISO), assuming a distance of 3.6 Mpc and an area coverage of  $14'' \times 27''$ . If we assume the same distance and coverage (the *west peak* would be left outside), the warm gas mass detected would be  $9.4 \times 10^6 M_\odot$ . Rigopoulou et al. (2002) estimate that the 2.5% of the gas in IC 342 is warm, using previous published data from Aalto et al. (1995) in various  $^{12}\text{CO}$ ,  $^{13}\text{CO}$  and  $\text{C}^{18}\text{O}$  transitions for the total molecular gas mass value, measured with a variety of telescopes. Using the same value for the total molecular gas mass (and correcting for the distance) we find that the percentage increases to 4.7%. Additionally, Mauersberger et al. (2003) report the 10% of the total molecular gas in IC 342 to be warm. Mauersberger et al. (2003) use the warm gas mass value reported by Rigopoulou et al. (2002) corrected for the assumed distance (1.8 Mpc), and compare it to the total molecular gas mass measured using  $^{13}\text{C}^{16}\text{O}$  data taken with the Heinrich-Hertz-Telescope. Assuming the same distance (1.8 Mpc) and amount of total molecular gas

mass than Mauersberger et al. (2003), and considering the three peaks, since the beam of Heinrich-Hertz-Telescope (34") covers all three of them, the amount of warm gas mass would be  $7.2 \times 10^5 M_{\odot}$ , which represents the 5.5% of the total molecular gas mass. In summary, using two different values for the total molecular gas mass (from Rigopoulou et al. (2002) and Mauersberger et al. (2003)), and two different area coverages, we still find that the percentage of warm gas mass to total molecular gas mass is  $\sim 5\%$ .

#### 4. Summary

We have imaged the nuclear region of IC 342 in  $\text{NH}_3(6,6)$  using the VLA. Three emission peaks are detected. The *(6,6) peak* corresponds well with GMC C and is probably a column density and temperature peak driven by a burst of star formation at the position where inflowing gas accumulates at a nuclear ring. The *continuum peak* is offset from GMCs B, N and A, but coincides with the 1.3 cm continuum peak. The 6 cm continuum peak is also very close, and due to the different resolution between the two maps, we can not rule out that the two peaks could be in fact coincident. The *continuum peak* is likely a temperature peak corresponding to very hot gas similar to the hot gas seen in our own Galactic Center around Sgr A\*. The *west peak* is a tentative detection with not known molecular or continuum emission counterpart. The fact that the *west peak* remains undetected in lower transition lines might be due to absorption along the line-of-sight, as is the case for the “high-line-ratio-cloud” in the Galactic Center. The presence of GMC N, as detected by Meier & Turner (2005), could not be positively confirmed in  $\text{NH}_3(6,6)$  emission.  $\text{NH}_3(6,6)$  emission above noise-level is detected at the position where this GMC has been reported. However, we did not detect a distinctive feature at this location.

We thank C.-W. Tsai and M. Lebrón for sharing their results in advance of publication. Thanks are also due to E. Schinnerer and D. Meier for providing the maps we have used for comparison and to T. Helfer for kindly answering all our questions regarding her results. During the development of this study, MM-C has been supported by an Academia Sinica Institute of Astronomy and Astrophysics (ASIAA) fellowship and a Smithsonian Institution Visiting Student Grant.

#### REFERENCES

Aalto, S., Booth, R.S., Black, J.H. & Johansson, L.E.B. 1995, A&A, 300, 369

- Becklin, E.E., Gatley, I., Mathews, K., Neugebauer, G. Sellgren, K., Werner, M.W. & Wynn-Williams, C.G. 1980, *ApJ*, 236, 441
- Beuther, H., Thorwirth, S., Zhang, Q., Hunter, T.R., Megeath, S.T., Walsh, A.J. & Menten, K.M. 2005, *ApJ*, 627, 834
- Böker, T., Förster-Schreiber, N.M. & Genzel, R. 1997, *AJ*, 114, 1883
- Böker, T., van der Marel, R.P. & Vacca, W.D. 1999, *ApJ*, 118, 831
- Downes, D., Radford, S.J.E., Guilloteau, S., Guélin, M., Greve, A. & Morris, D. 1992, *A&A*, 262, 424
- Helfer, T.T. & Blitz, L. 1993, *ApJ*, 419, 86
- Helfer, T.T., Thornley, M.D., Regan, M.W., Wong, T., Sheth, K., Vogel, S.N., Blitz, L. & Bock, D.C.-J. 2003, *ApJS*, 145, 259
- Henkel, C., Mauersberger, R., Peck, A.B., Falcke, H. & Hagiwara, Y. 2000, *A&A*, 361, L45
- Herrnstein, R.M. & Ho, P.T.P. 2002, *ApJ*, 579, L83
- Herrnstein, R.M. 2003, Ph.D Thesis, Harvard University
- Herrnstein, R.M. & Ho, P.T.P. 2005, *ApJ*, 620, 287
- Ho, P. T. P., Martin, R. N., & Ruf, K. 1982, *A&A*, 113, 155
- Ho, P.T.P. & Martin, R.N. 1983, *ApJ*, 272, 484
- Ho, P.T.P., Turner, J.L. & Martin, R.N. 1987, *ApJ*, 322, L67
- Ho, P.T.P., Martin, R.N., Turner, J.L. & Jackson, J.M. 1990, *ApJ*, 355, L19
- Hüttemeister, S., Wilson, T.L., Bania, T.M. & Martín-Pintado, J. 1993, *A&A*, 280, 255
- Hüttemeister, S., Henkel, C., Mauersberger, R., Brouillet, N., Wiklind, T. & Millar, T. J. 1995, *A&A*, 295, 571
- Ishizuki, S., Kawabe, R., Ishiguro, M., Okumura, S.K., Morita, K.I., Chikada, Y. & Kasuga, T. 1990, *Nature*, 344, 224
- Israel, F.P. & Baas, F. 2003, *A&A*, 404, 495
- Jackson, J.M., Heyer, M., Paglione, T.A.D. & Bolatto, A.D. 1996, *ApJ*, 456, L91

- Karachentsev, I.D. 2005, ApJ, 129, 178
- Lo, K.Y., Berge, G.L., Claussen, M.J., Heiligman, G.M., Leighton, R.B., Masson, C.R., Moffet, A.T., Phillips, T.G., Sargent, A.I., Scott, S.L., Wannier, P.G. & Woody, D.P. 1984, ApJ, 282, L59
- Martin, R.N. & Ho, P.T.P. 1979, A&A, 74, L7
- Martin, R.N. & Ho, P.T.P. 1986, ApJ, 308, L7
- Mauersberger, R., Henkel, C., Weiß, A., Peck, A.B. & Hagiwara, Y. 2003, A&A, 403, 561
- Meier, D.S., Turner, J.L. & Hurt, R.L. 2000, ApJ, 531, 200
- Meier, D.S. & Turner, J.L. 2001, ApJ, 551, 687
- Meier, D.S. & Turner, J.L. 2005, ApJ, 618, 259
- Ott, J., Weiss, A., Henkel, C. & Walter, F. 2005, ApJ, 629, 767
- Rigopoulou, D., Kunze, D., Lutz, D., Genzel, R. & Moorwood, A.F.M. 2002, A&A, 389, 374
- Saha, A., Claver, J. & Hoessel, J.G. 2002, AJ, 124, 839
- Schinnerer, E., Böker, T. & Meier, D.S. 2003, ApJ, 591, L115
- Schulz, A., Gürsten, R., Köster, B. & Krause, D. 2001, A&A, 371, 25
- Takano, S., Nakai, N. & Kawaguchi, K. 2002, PASJ, 54, 195
- Turner, J.L., Hurt, R.L. & Hudson, D.Y. 1993, ApJ, 413, L19
- Turner, J. L., & Hurt, R. L. 1992, ApJ, 384, 72
- Turner, J.L. & Ho, P.T.P. 1983, ApJ, 268, L79
- Weiß, A., Neininger, N., Henkel, C., Stutzki, J. & Klein, U. 2001, ApJ, 554, L143
- Womack, M. Ziurys, L.M. & Wyckoff, S. 1992, ApJ, 393, 188

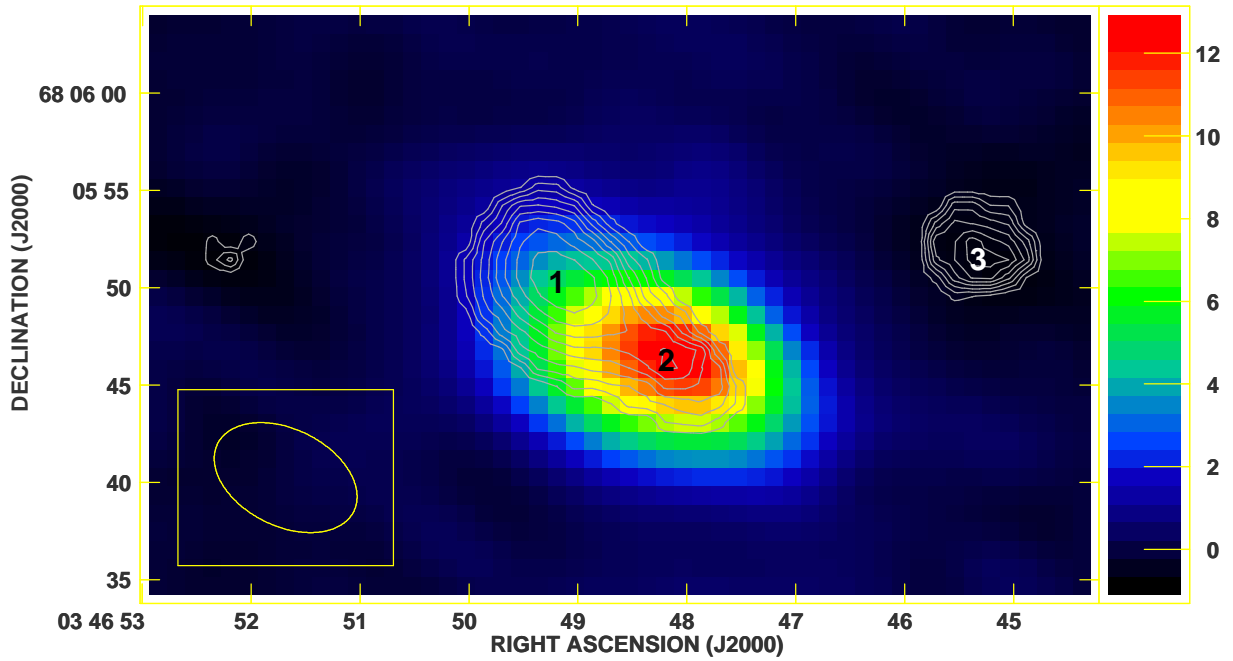


Fig. 1.—  $\text{NH}_3(6,6)$  integrated intensity map. The contours represent the line emission, while the false-color scale indicates the continuum emission at 1.3 cm. Peak 1 represents the  $(6,6)$  peak, peak 2 the *continuum peak* and peak 3 the *west peak*. The contour levels are in steps of 10% of the intensity peak, from 5.5 mJy Beam<sup>-1</sup> km s<sup>-1</sup> to 49.5 mJy Beam<sup>-1</sup> km s<sup>-1</sup>. The RMS is 3.6 mJy Beam<sup>-1</sup> km s<sup>-1</sup>, therefore the contour levels in the map are in steps of  $\sim 1.5 \sigma$ , from  $1.5 \sigma$  to  $13.7 \sigma$ . The false-color scale is in mJy Beam<sup>-1</sup>.



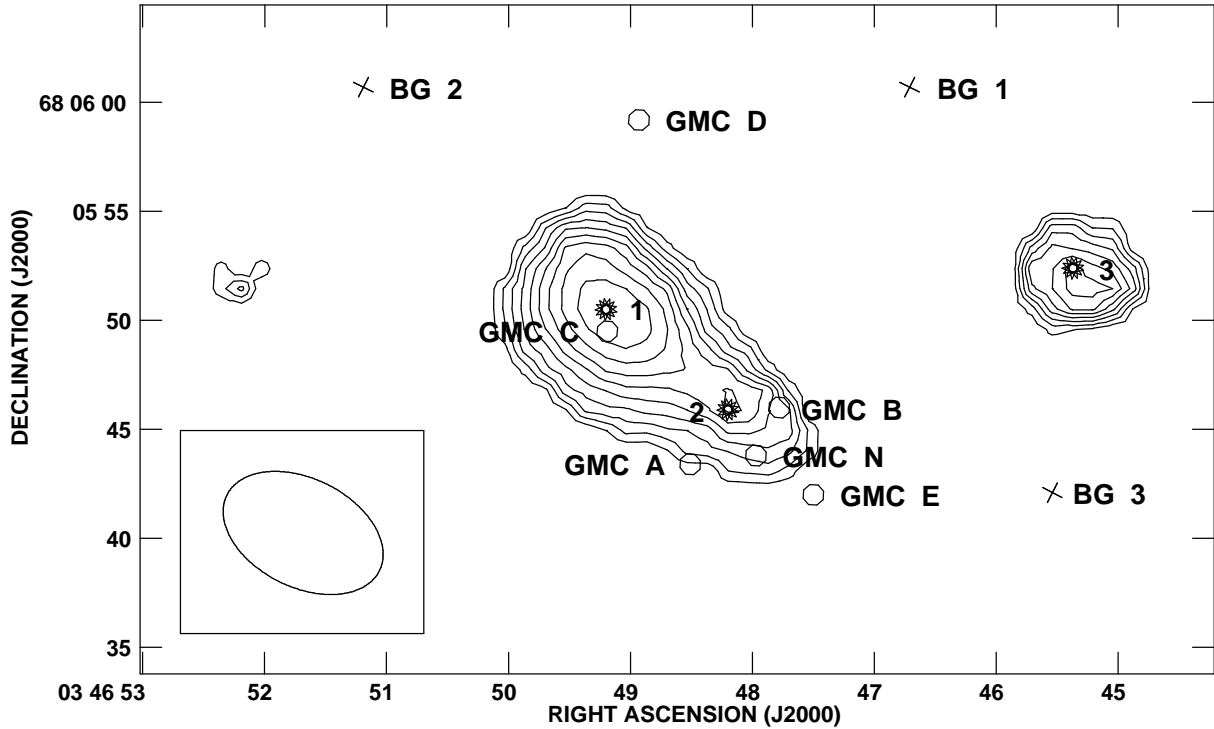


Fig. 2.—  $\text{NH}_3(6,6)$  integrated intensity map. We have marked the positions of the three  $\text{NH}_3(6,6)$  detected peaks as well as those of the 6 GMCs as described by Downes et al. (1992) and Meier & Turner (2005). The 6 GMCs are marked with circles, the  $(6,6)$  peak (peak 1), the *continuum peak* (peak 2) and the *west peak* (peak 3) are marked with stars and numbers. We have also marked three random background positions whose spectra we have plotted (figure 3) for comparison reasons. The background points are marked with crosses and labeled 'BG1', 'BG2' and 'BG3'.

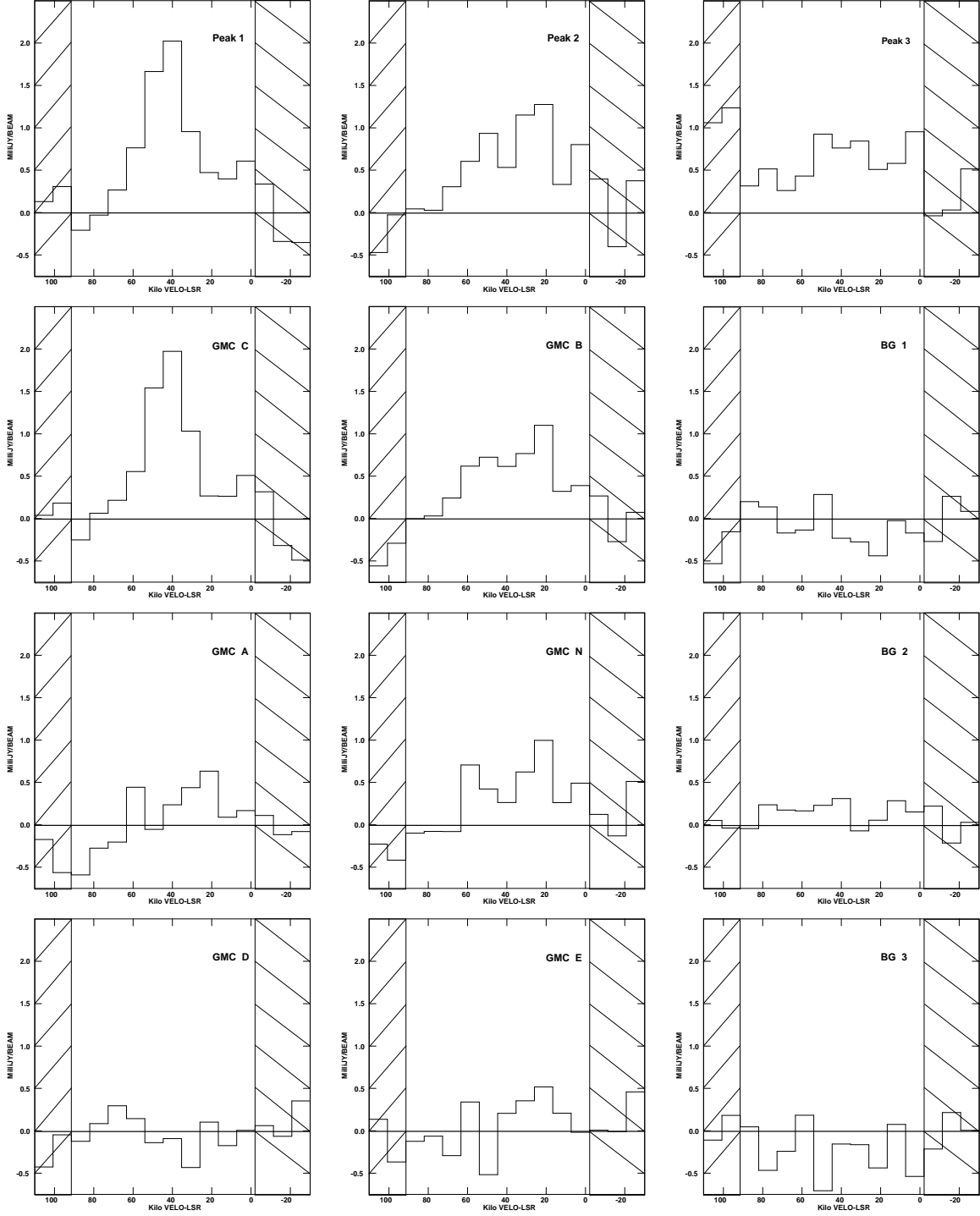


Fig. 3.— Spectra measured at the positions of the 6 GMCs (GMCs A, B, C, D, E and N), the three peaks detected in  $\text{NH}_3(6,6)$  (peaks 1,2 and 3 from figure 2) and three random background positions (BG1, BG2 and BG3). The shaded areas represent the channels we have either removed because their noise level is too high (channels 1, 14 and 15), which correspond to velocities from  $-30$  to  $-20$   $\text{km s}^{-1}$  and from  $-90$  to  $+110$   $\text{km s}^{-1}$ , or used for continuum subtraction (channels 2 and 3, velocity from  $-20$  to  $\sim 0$   $\text{km s}^{-1}$ ).

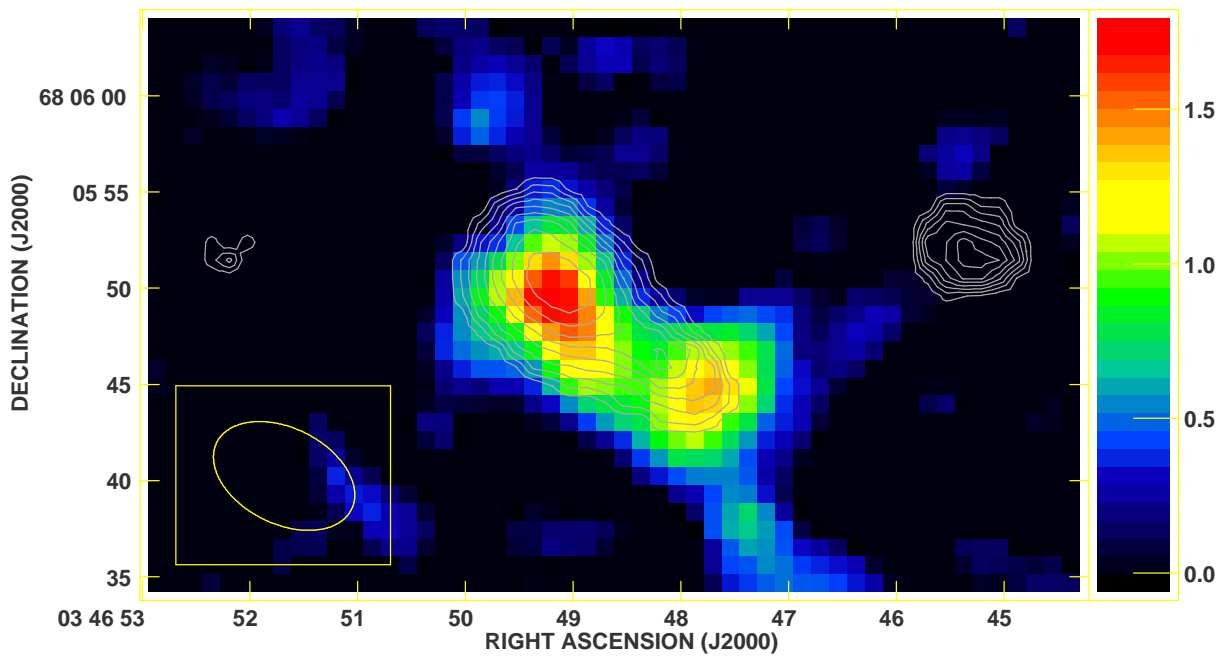


Fig. 4.—  $\text{NH}_3(6,6)$  integrated intensity in contours.  $\text{HC}_3\text{N}(10-9)$  integrated intensity in false-color scale. Contour levels are as in figure 1. The false-color scale is in  $\text{mJy Beam}^{-1} \text{ km s}^{-1}$  (Meier & Turner 2005).

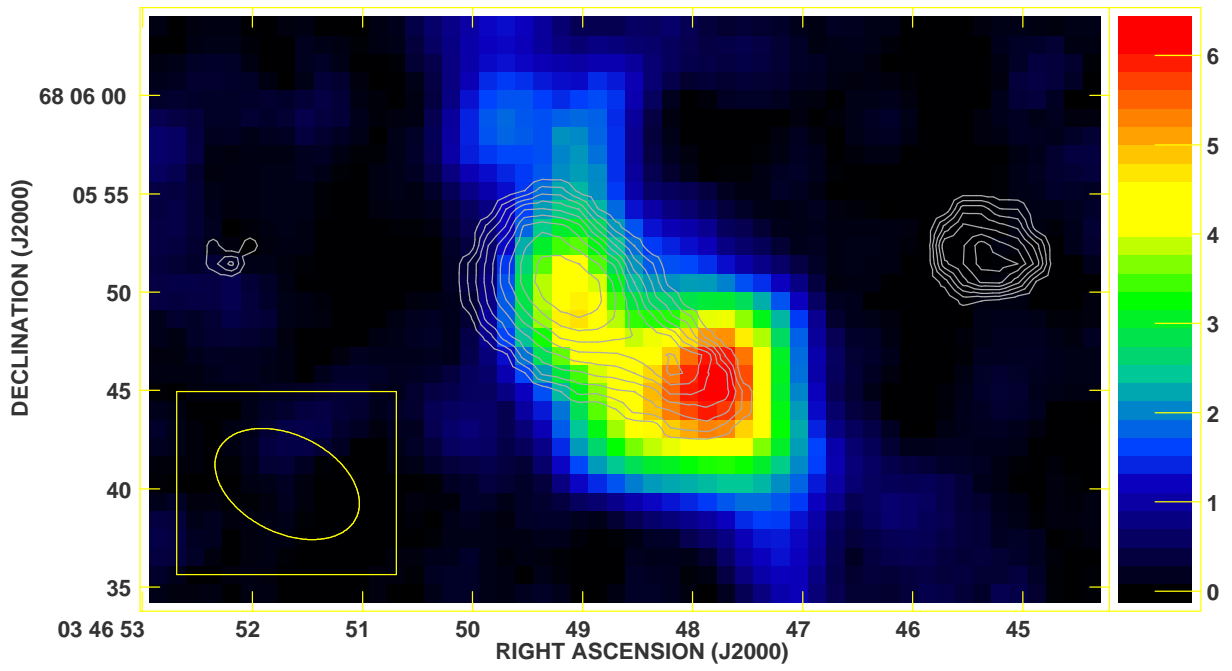


Fig. 5.—  $\text{NH}_3(6,6)$  integrated intensity in contours.  $\text{HNC}(1-0)$  integrated intensity in false-color scale. Contour levels are as in figure 1. The false-color scale is in  $\text{mJy Beam}^{-1} \text{ km s}^{-1}$  (Meier & Turner 2005).

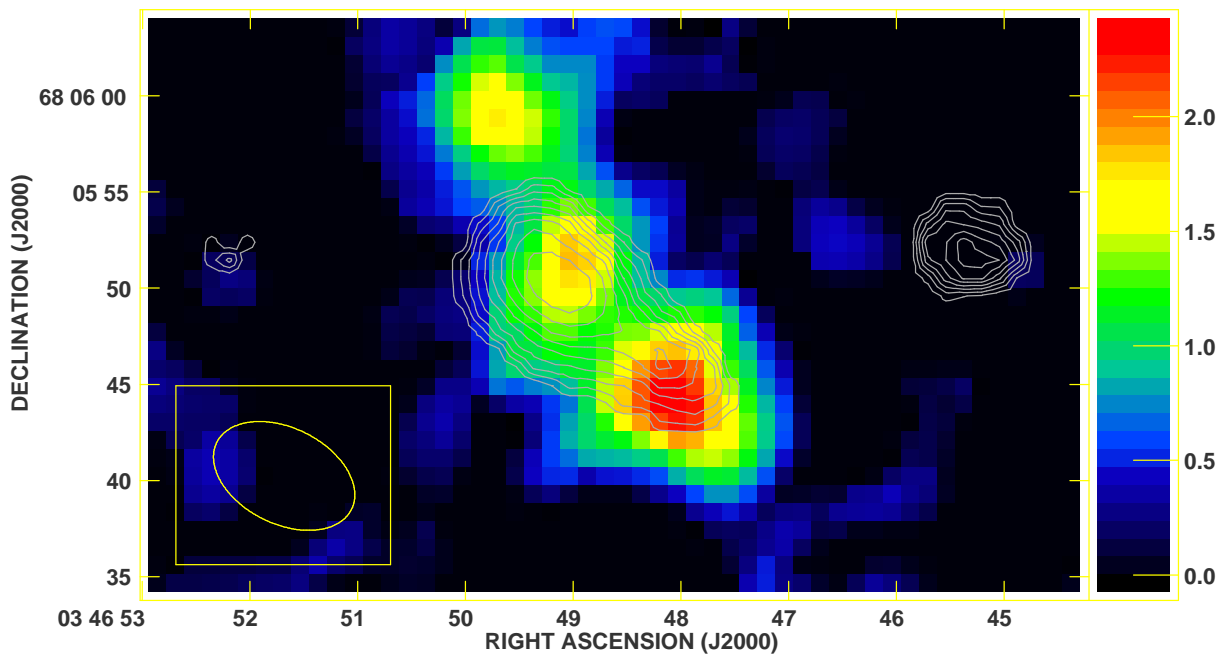


Fig. 6.—  $\text{NH}_3(6,6)$  integrated intensity in contours.  $\text{N}_2\text{H}^+(1-0)$  integrated intensity in false-color scale. Contour levels are as in figure 1. The false-color scale is in  $\text{mJy Beam}^{-1} \text{ km s}^{-1}$  (Meier & Turner 2005).

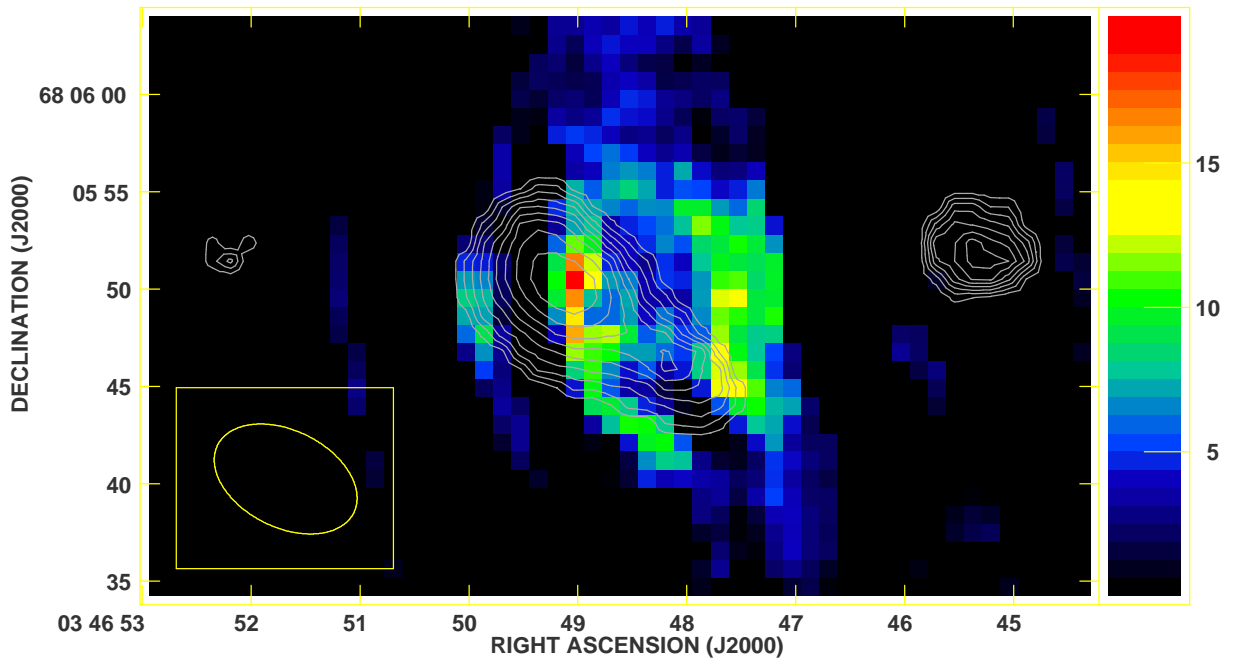


Fig. 7.—  $\text{NH}_3(6,6)$  integrated intensity in contours.  $\text{CO}(2-1)$  integrated intensity is in false-color scale and traces the eastern and western parts of the molecular ring. Contour levels are as in figure 1. The false-color scale is in  $\text{mJy Beam}^{-1} \text{ km s}^{-1}$  (Schinnerer et al. 2003).

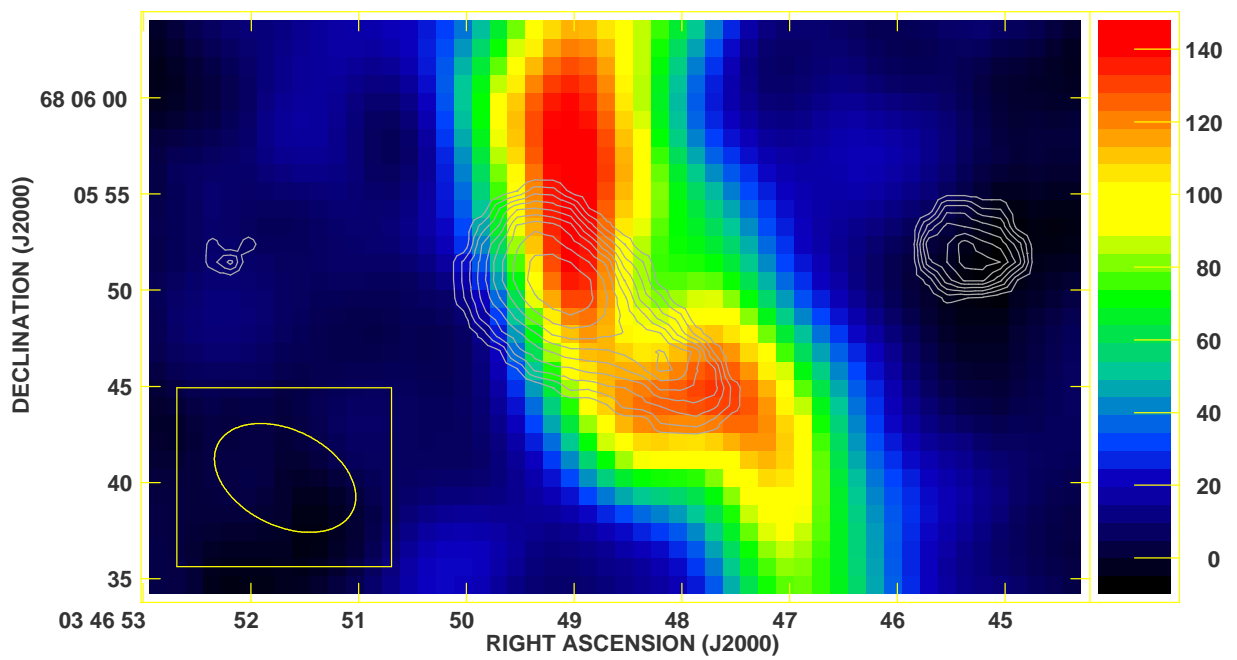


Fig. 8.—  $\text{NH}_3(6,6)$  integrated intensity in contours.  $\text{CO}(1-0)$  integrated intensity is shown in false-color scale, and traces the mini-spiral. Contour levels are as in figure 1. The false-color scale is in  $\text{mJy Beam}^{-1} \text{ km s}^{-1}$  (Helfer et al. 2003).

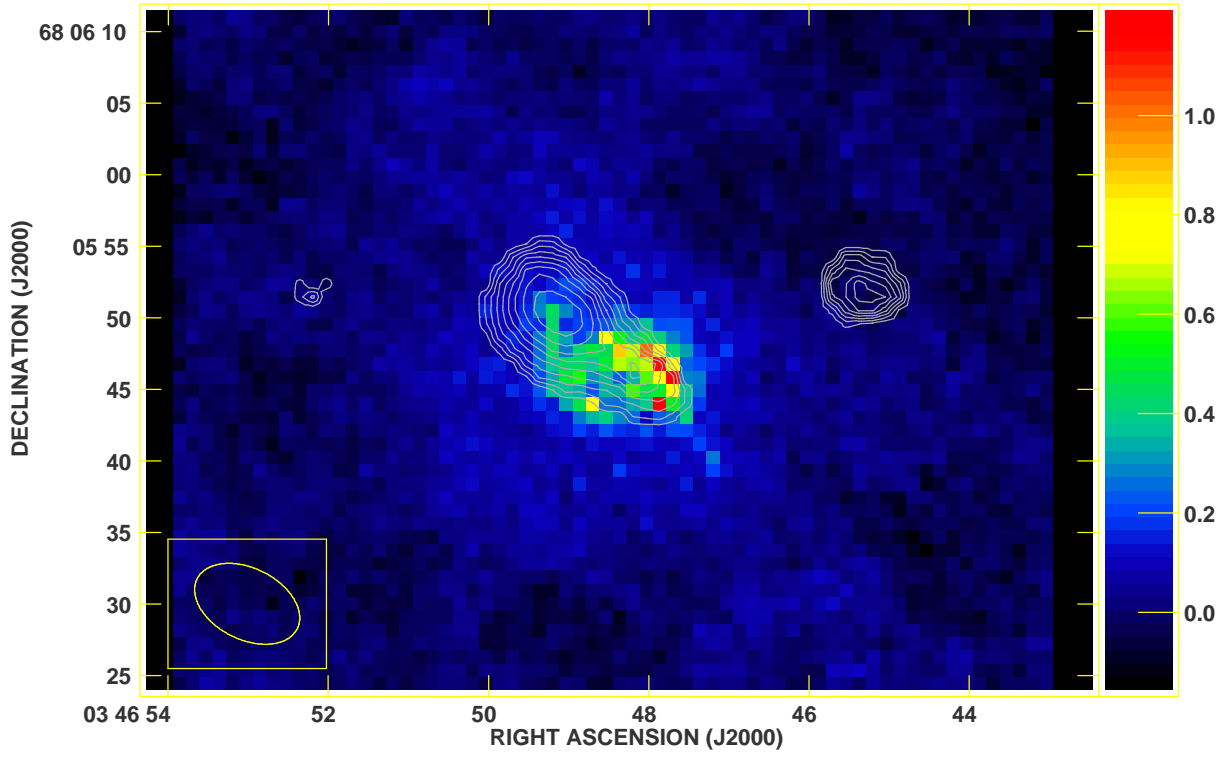


Fig. 9.—  $\text{NH}_3(6,6)$  integrated intensity in contours. VLA 6 cm continuum integrated intensity in false-color scale. Contour levels are as in figure 1. The false-color scale is in  $\text{mJy Beam}^{-1}$ .



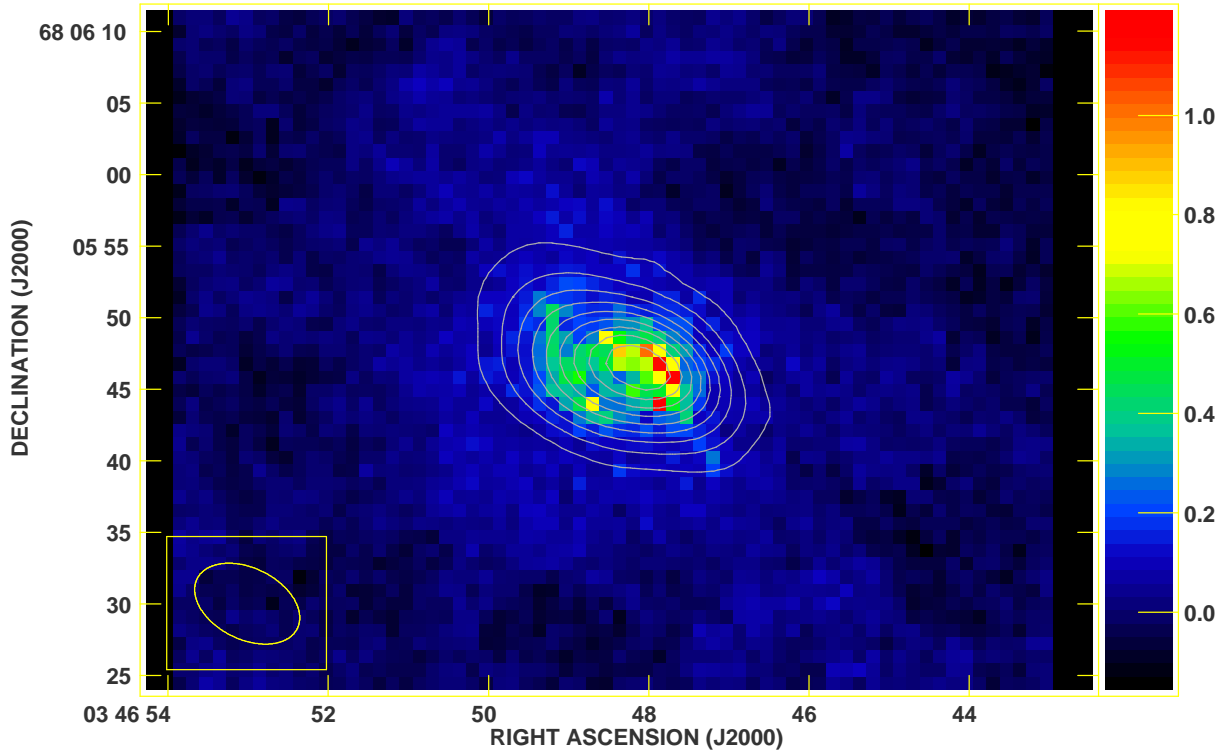


Fig. 10.— 1.3 cm continuum integrated intensity in contours. VLA 6 cm continuum integrated intensity in false-color scale. Contour levels are in steps of 10% of the continuum intensity peak, from  $13 \text{ mJy Beam}^{-1}$  to  $114 \text{ mJy Beam}^{-1}$ . The false-color scale is also in  $\text{mJy Beam}^{-1}$ .

Table 1: Calculated warm masses for the three detected peaks for a distance of 3.3 Mpc.

Peak	Line flux $10^{-3}$ Jy Beam $^{-1}$	$T_b$ K	$\Delta v$ km s $^{-1}$	$N_{66}$ $10^{13}$ cm $^{-2}$	Area $10^4$ pc $^2$	$M_{H_2}$ $10^6 M_\odot$
<i>(6,6) peak</i>	2.1	0.12	40	3.7	2.6	4.8
<i>Continuum peak</i>	1.4	0.08	50	3.1	1.2	1.8
<i>West peak</i>	1.1	0.06	80	4.0	0.8	1.6